



Implantable, wireless, self-fixing thermal sensors for continuous measurements of microvascular blood flow in flaps and organ grafts

Di Lu^{a,1}, Shupeng Li^{b,1}, Quansan Yang^{a,b}, Hany M. Arafa^{a,c}, Yameng Xu^d, Ying Yan^e, Diana Ostojich^a, Wubin Bai^a, Hexia Guo^{a,f}, Changsheng Wu^a, Shuo Li^a, Lauren Jacobson^g, Amanda M. Westman^g, Matthew R. MacEwan^e, Yonggang Huang^{a,b,f,h,*}, Mitchell Pet^{g,**}, John A. Rogers^{a,b,c,f,i,j,k,***}

^a Querrey Simpson Institute for Bioelectronics, Northwestern University, Evanston, IL, 60208, USA

^b Department of Mechanical Engineering, Northwestern University, Evanston, IL, 60208, USA

^c Department of Biomedical Engineering, Northwestern University, Evanston, IL, 60208, USA

^d The Institute of Materials Science and Engineering, Washington University in St. Louis, St. Louis, MO, 63130, USA

^e Department of Neurological Surgery, Washington University School of Medicine, St Louis, MO, 63110, USA

^f Department of Materials Science and Engineering, Northwestern University, Evanston, IL, 60208, USA

^g Department of Plastic and Reconstructive Surgery, Washington University School of Medicine, St Louis, MO, 63110, USA

^h Department of Civil and Environmental Engineering, Northwestern University, Evanston, IL, 60208, USA

ⁱ Department of Neurological Surgery, Feinberg School of Medicine, Northwestern University, Chicago, IL, 60611, USA

^j Department of Electrical and Computer Engineering, Northwestern University, Evanston, IL, 60208, USA

^k Department of Chemistry, Weinberg College of Arts and Sciences, Northwestern University, Evanston, IL, 60208, USA

ARTICLE INFO

Keywords:

Implantable wireless devices
Flow sensing
Biodegradable materials
Heat convection
Thrombosis diagnosis

ABSTRACT

Vascular pedicle thrombosis after free flap transfer or solid organ transplantation surgeries can lead to flap necrosis, organ loss requiring re-transplantation, or even death. Although implantable flow sensors can provide early warning of malperfusion and facilitate operative salvage, measurements performed with existing technologies often depend on extrinsic conditions such as mounting methods and environmental fluctuations. Furthermore, the mechanisms for fixing such probes to vascular or skeletal structures may disrupt the normal blood flow or cause unnecessary tissue damage. Requirements for wired connections to benchtop readout systems also increase costs, complicate clinical care and constrain movements of the patient. Here, we report a wireless, miniaturized flow sensing system that exploits sub-millimeter scale, multi-nodal thermal probes, with biodegradable barbs that secure the probes to the surrounding tissues in a manner that facilitates removal after a period of use. These smartphone-readable devices, together with experimentally validated analytical models of the thermal transport physics, enable reliable, accurate flow sensing in ways that are largely immune to variations in temperature and mechanical perturbations. In vivo demonstrations of this technology in porcine myocutaneous flap and kidney malperfusion models highlight the essential capabilities in microsurgical and transplantation-related biomedical application scenarios.

1. Introduction

Vascularized free tissue auto- or allotransplantation is the ultimate means to treat the loss or dysfunction of a vital body part. For example, autologous free flaps replace areas of missing tissue after traumatic

injury or oncologic resection, while allotransplanted kidneys and livers can be lifesaving in cases of total organ failure. Each of these reconstructive procedures depends upon the successful transfer of tissue from one site to another, with re-establishment of tissue circulation by repair of the critical artery and vein(s) at the recipient site. Thrombosis (blood

* Corresponding author. Querrey Simpson Institute for Bioelectronics, Northwestern University, Evanston, IL, 60208, USA.

** Corresponding author.

*** Corresponding author. Querrey Simpson Institute for Bioelectronics, Northwestern University, Evanston, IL, 60208, USA.

E-mail addresses: y.huang@northwestern.edu (Y. Huang), mpet@wustl.edu (M. Pet), jrogers@northwestern.edu (J.A. Rogers).

¹ These authors contributed equally to this work.

clotting) at the site of these critical vascular anastomoses is one of the most common modes of early post-operative failure. For example, venous and/or arterial thrombosis occurs in 5–10% flaps, as the primary failure mechanism (Askari et al., 2006; Chen et al., 2007; Novakovic et al., 2009); 76–91% of the thrombosis appears within 48 h of the surgery, rising to 94–97% after a week (Chen et al., 2007; Kroll et al., 1996). Renal arterial or venous thrombosis is a major cause of graft loss in the early (<1 week) post-surgical period (Kobayashi et al., 2007). Hepatic arterial thrombosis is the second main cause of liver graft failure (Pareja et al., 2010). Due to the risk of hemorrhage, there is a fundamental limitation in the use of anti-clotting drugs after surgery, demanding alternative methodologies for the timely diagnosis of thrombosis in these cases. Clinically convenient and cost-effective methods for rapid detection of thrombosis throughout the critical risk period could greatly improve the care of these patients.

Microsurgical free flap monitoring historically has relied upon on empirical, qualitative methods such as observations of tissue color, tests of bleeding rate after a pin prick, and intermittent Doppler examination (Hirigoyen et al., 1995; Spiegel and Polat, 2007). More recently, strategies for continuous monitoring have been developed including implantable Doppler probes which wrap around the pedicle vessels, and near-infrared spectroscopy (NIRS) techniques that detect cutaneous tissue oxygen saturation (StO₂) (Keller, 2007, 2009). While these continuous strategies have facilitated expeditious identification of flap thrombosis and improved salvage rates, each remains substantially limited. Implantable Doppler devices may yield results subject to inconsistent interpretation due to mounting methods (Poder and Fortier, 2013); the wired connection between the delicate flap pedicle vessels and the external readout system also risks iatrogenic vascular disruption or kinking in the post-operative period as well as during removal (Khot et al., 2005). Peripherally mounted cutaneous NIRS probes obviate such risks, yet these devices are still wired, restricting movements of patients, and creating the potential for mechanical damage and motion artifacts. Such devices are also inapplicable to muscle flaps and buried flaps which lack the required skin paddle (Kozusko and Gbulie, 2018).

While occurring in distinct clinical situations, the task of monitoring solid organ allotransplantation shares many challenges and potential solutions with microvascular free flap monitoring. In this case, the pedicle vessels are larger, and thrombosis is less common, but the consequences of organ ischemia and loss can be even more devastating. Buried in the thorax, peritoneum, or retroperitoneum, solid organ transplants are difficult to directly monitor. Intermittent Doppler duplex ultrasound is currently the main diagnostic method to identify the anastomosed arteries and veins extracorporeally, and to determine the vascular flow velocities (Lorenzetti et al., 1999; Spiegel and Polat, 2007). Deploying implantable Doppler probes for continuous measurements yields unsatisfactory results, as such sensors only detect vascular occlusions of a single monitored vessel but not all anastomosed vessels connected to the organ (Amdisen et al., 2017).

An ideal probe for monitoring both microsurgical flaps and transplanted organs should be wireless, continuous, sensitive to cessation of both arterial and venous flow, applicable to both muscle and skin flaps in addition to organs, robust to variations in tissue type, operable in a location remote from the delicate pedicle vessels, mechanically stable within the target tissue, and easy/safe to remove. Implantable thermal microvascular flow probes have several advantages including the capability of operating within almost any soft tissue and the lack of a need to contact the source vessels. Indeed, thermal models established previously guide the design of thermal probes for measuring the thermal conductivity and diffusivity (Arkin et al., 1994; Baish, 2015; Chen et al., 1981; Diller, 2017; Valvano et al., 1985), yielding accurate perfusion values for ex vivo tissues and organs (Anderson et al., 1992; Valvano et al., 1984). In vivo thermal probes such as those for intracranial thermal microvascular flow sensing also exists for the continuous monitoring of cerebral perfusion (Rosenthal et al., 2011). However, such devices involve hard wired interfaces to external measurement

equipment, and they demand semi-permanent skeletal mounting to achieve mechanical stability sufficient for accurate results in vivo (Rosenthal et al., 2011). This latter requirement complicates the surgery processes, causes unnecessary damage to adjacent skeletal structures, and creates difficulties in removal. Moreover, the observed high levels of baseline drifts (likely due to thermal fluctuations in the environment and remnant mechanical disturbances) in such in vivo probes lead to difficulties in distinguishing normal and thrombotic phases, thereby limiting uses in clinical practice (Jaeger et al., 2005). Additionally, the heaters in the previous probes, as well as the discussion in the corresponding thermal models, confine themselves to 3-dimensional (3D) spherical cases, but not other heater shapes (Khot et al., 2005; Valvano et al., 1984); fixing this degree of freedom also limits the ability for tuning the sensitivity of the sensors. These thermal models do not include microscopic quantities such as flow velocity (Baish, 2015), which can be directly observed by imaging methods; modeling and calculating such velocity values would provide a direct comparison as a further evidence of the accuracy for the flow measurements.

Recently reported classes of soft, biomedical electronic sensors that exploit Bluetooth data acquisition and wireless transmission modules provide attractive means for eliminating the necessity of bulky measurement equipment and hard-wired tethers. Previous examples include various skin-interfaced devices such as mechano-acoustic sensors of various physiological processes and body motions (Lee et al., 2020), vital signs monitoring systems for neonatal and pediatric intensive-care units (Chung et al., 2020; Rwei et al., 2020), skin hydration sensors for inflammatory skin diseases (Kwon et al., 2021; Madhupathy et al., 2020), catheter-type oximeters for cardiac oxygen saturation (Lu et al., 2021), and pressure sensors for compression therapy (Park et al., 2020). These devices typically combine a sensor sub-system with a flexible wireless module that gently but firmly mounts onto the surface of the skin using a standard, double-sided biomedical adhesive, for continuous measurements that can occur over extended periods of time.

Biodegradable structural materials have relevance to the sensor component of the systems considered here, as a convenient means for temporary mechanical fixation of the probe to the surrounding soft tissues. After some desired operational period, these materials degrade and disappear into benign products soluble in physiological environments, ultimately resorbed into the body. Demonstrations of related mechanisms in other contexts include bonding with biodegradable adhesives (Bhagat and Becker, 2017), binding with biodegradable sutures (Seitz et al., 2015), and supporting frameworks with stents or scaffolds (Wykrzykowska et al., 2017). Recent research also suggests that biodegradable materials may help to avoid pathogenic film deposition on devices or inflammatory responses of the surrounding tissues for long-term implantation (Kang et al., 2016; Yu et al., 2016).

The work described here combine these materials, wireless capabilities, as well as considerations about the related physical models and designs into thermal flow sensing probes that enable early and reliable detection of arterial and/or venous thrombosis in muscle free flaps and allotransplanted solid organs. The system contains a miniaturized, implantable sensor based on thermal transport for microvascular flow measurements with a biodegradable fixation structure, which interfaces to a small Bluetooth low energy (BLE) data communication module that adheres to the skin (Fig. 1a). Multiple temperature sensing nodes integrated onto the probe exploit designs optimized through computational modeling to minimize parasitic thermal transport and to include 2-dimensional (2D), adjustable heaters for accurate, highly sensitive measurements. The total dimensions are slightly smaller than those of a #12 biopsy needle (~2 mm diameter), to allow for minimally invasive insertion. Biodegradable barbs serve as a cladding layer that stabilizes the probes in soft tissues, with a simple implantation process that consists of inserting the probe into an incision formed with a scalpel. In vitro studies indicate that barbs retain mechanical stability for up to ~9 days, after which their mechanical properties degrade to allow removal with a small extraction force. A BLE module enables wireless communication as

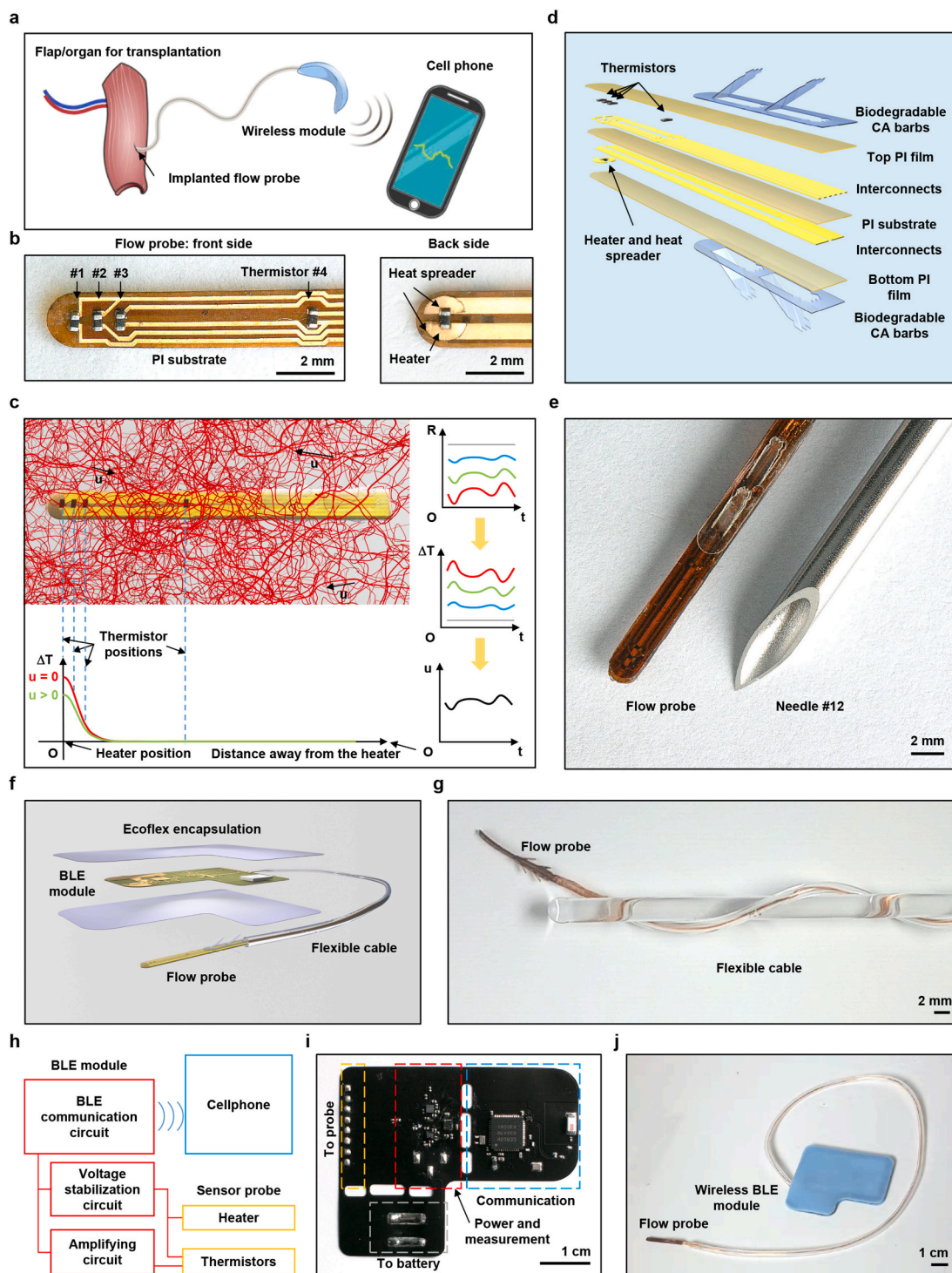


Fig. 1. a) Schematic illustration of the microvascular flow measurement system. b) Sensing components in a flow probe. c) top-left, schematic illustration of a flow probe implanted in tissue (network of microvascular blood vessels is also shown); bottom-left, schematic illustration of the temperature distribution with and without the presence of the microvascular flow of velocity u ; right, flow chart of the signal conversion process. d) Exploded view schematic illustration of a flow probe. e) Photograph of a fabricated flow probe; the dimensions are comparable to those of a biopsy needle. f) Schematic illustration of the complete flow sensor, showing an exploded view of the BLE module. g) Photograph of a flow probe and its flexible cable. h) Schematic block diagram of the circuits of the BLE module. i) Photograph of a BLE module. j) Photograph of an assembled flow sensor.

well as real-time monitoring of the flow, via a standard smartphone as a cost-effective platform for data display, storage and processing through an intuitive graphical user interface. In vivo studies that involve implantation into porcine myocutaneous microvascular flap and kidney transplant models demonstrate quantitative, accurate measurements of flow. In addition to the typical parameter (tissue perfusion) to describe

microvascular flow, we also report modeling and the measurement results for flow velocity, a physical quantity that can be directly compared with flow values measured in other methods as well as in benchtop experiments. These findings suggest that such devices may act as accurate, convenient, and low-cost platforms for timely detection of post-surgical thrombosis in transplanted tissues and organs.

The sensing components consist of a surface-mount resistive heater and four (#1-#4) surface-mount negative temperature coefficient (NTC) thermistors at different relative positions along the length of the probe (Fig. 1b and c). Inert, biocompatible traces of noble metals (Au/Pt, 50/300 nm) on a polyimide substrate (PI, 75 μm) form interconnects to these components. Compared with previous thermal-based single-nodal flow sensors implemented with wires of macroscopic cross-sectional areas (Khot et al., 2005), the thin, narrow geometries of the metal traces defined by laser patterning in the designs reported here minimize thermal transport through the metal, thereby significantly improving the sensitivity to the thermal properties of the surrounding tissue. The use of multiple temperature sensing nodes further reduces the error in the flow measurements via least-square fitting. A circular gold film (diameter 1.5 mm, thickness 25 μm) around the heater spreads the heat evenly in a well-defined circular shape. An alternative configuration uses Au/Pt (50/300 nm) thin film resistors instead of surface-mount components, as a probe based only on noble metals for the functional elements to further reduce the size and to improve the biocompatibility (Fig. S1), with reduced temperature sensitivity and increased error of flow velocity. Encapsulating the top and bottom sides of the probe with PI ensures stable operation in biofluids. Biodegradable barbs temporarily fix the probe to the target tissue location (Fig. 1d). The cross-sectional dimensions of the probe (2 mm width \times 1 mm thickness) are smaller than those of biopsy needles (12-gauge, Fig. 1e).

Insulated copper wires sealed in flexible silicone tubing connect the probe to a silicone-encapsulated BLE module (Fig. 1f and g). A voltage stabilizer circuit supplies power to the heater through the copper wires and the noble metal interconnects. Wheatstone bridges and amplifiers connected to the NTC thermistors enable accurate sensing of their resistances, and therefore, the temperatures at the target locations (measurement error ~ 0.06 $^{\circ}\text{C}$). An Android cellphone with a custom app serves as a user interface (Methods section, Fig. 1h and i) for controlling the operation of the heater and for acquiring temperature data in real-time. Fig. 1j shows the fully assembled sensor system.

2. Methods

2.1. Fabrication of flow probes

Sequentially depositing Cr (10 nm, adhesion layer), Pt (300 nm) and Au (50 nm) by electron beam evaporation formed conductive films on both sides of PI substrates (75 μm). Laser-ablating and cutting (U laser, LPKF Laser & Electronics) these substrates, bare PI sheets (75 μm), gold foils (25 μm) and CA films (250 μm) yielded metal interconnects, PI encapsulation structures, heat spreaders and CA barbs (manual bending by tweezers formed the $\sim 30^{\circ}$ angle between the barbs and the CA film), respectively. PI encapsulation prevents the penetration of conductive biofluids, avoiding short circuit. Lead-free solder (Sn/Bi/Ag) formed electrical interfaces between the Au/Pt interconnects and the surface-mount components (footprint 0201, heater resistance 1.1 k Ω , thermistor resistance 10 k Ω , thermistor $B = 3380$), as well as from the interconnects to the copper wires. Assembling the individual parts by applying epoxy between the layers completed the fabrication.

2.2. Design and fabrication of BLE modules

A non-conductive epoxy (Loctite 3621, Henkel) mechanically bonded the surface mount components to the flexible printed circuit board (fPCB, PCBway) and reflow soldering with low-temperature solder paste (4900P SAC305, MG Chemicals) established electrical contact between the surface mount components and the copper pads on the fPCB. The design of the BLE modules as well as the Android App follows the method in previous reports (Krishnan et al., 2020). Compact lithium batteries (Lipo LP501522, 200 mA h) powered the BLE module for wireless communication.

2.3. Theory of flow sensing and verification

Theoretical modeling of the thermal physics establishes a quantitative understanding of the various effects and provides guidelines for optimized layouts. The temperature measured by the device is strongly affected by heat transfer in the tissue (and biofluid, primarily blood) and fluid flow in microchannels or microvascular blood vessels (Fig. 1c) as fluid flow carries heat away from the heater, effectively reducing the heat flux into the tissue. Let q denote the heat flux of the heater, and q' (to be determined) the effective heat flux for heat conduction into the tissue (and biofluid). Their difference is the heat carried away by fluid flow via heat convection (Supplementary Note 1, Figs. S2a and b), i.e.,

$$q\pi R^2 = q'\pi R^2 + q''S_{\text{vessels}}, \quad (1)$$

where πR^2 is the area of the spreader (heater) with radius R , $q''S_{\text{vessels}}$ is the heat carried away by fluid flow, q'' (to be determined) is the corresponding heat flux which vanishes for stationary fluid (zero flow velocity), and the net area of microvascular blood vessels S_{vessels} under the heater is related to blood content s (volume fraction of blood, or channel volume fraction for in-vitro experiments) by $S_{\text{vessels}} = s\pi R^2$. Equation (1) then becomes $q = q' + sq''$. The temperature change on the flap surface ΔT is related to q' via a heat conduction model of a semi-infinite solid (without the fluid) subjected to surface heat flux q' over a circle of radius R (Supplementary Note 1) (Carslaw and Jaeger, 1959). ΔT is also related to q'' by a boundary layer convection problem with fluid flow and flow velocity u (Supplementary Note 1) (Bergman et al., 2011). These, combined with Equation (1), give

$$\Delta T \approx \frac{qR/k}{1 + 0.76s\sqrt{\frac{uR}{\alpha_{\text{fluid}}}}} F\left(\frac{r}{R}\right), \quad (2)$$

where k is the effective thermal conductivity of the tissue, α_{fluid} is the thermal diffusivity of the fluid, $F\left(\frac{r}{R}\right) = \int_0^{\infty} J_0(\lambda r)J_1(\lambda R) \frac{d\lambda}{\lambda}$ (Fig. S2c), J_0

and J_1 are Bessel functions of the first kind for integer orders of 0 and 1, respectively, and r is the distance to the center of the heater. The above model accounts for both heat transfer and fluid flow simultaneously. For representative parameters in experiments, the ratio $\frac{sq''}{q}$ is $\sim 40\%$ for in-vivo experiments, which highlights the importance of accounting for the heat carried away by fluid flow. Equation (2) relates the surface temperature measured by the devices to the flow velocity u , and therefore establishes the method to determine u . Perfusion w is related to the flow velocity u by

$$w = \frac{uA_{\text{vessels}}}{V}, \quad (3)$$

where A_{vessels} is effective total cross-sectional area of the microvascular blood vessels (Supplementary Note 1) and V is total volume of the flap.

2.4. Error analysis of the results

Differentiating formula (2) gives an estimation of the error of the flow velocity:

$$\frac{\delta u}{u} = -2 \frac{\delta \Delta T}{\Delta T} \left/ \left(1 - \frac{1}{1 + 0.76s\sqrt{uR/\alpha}} \right) \right. - 2 \frac{\delta s}{s}, \quad (4)$$

where δ denotes the estimation of the errors of the corresponding quantities: $\delta \Delta T / \Delta T$ denotes the relative measurement error of the temperature, $\delta s / s$ denotes the relative uncertainty of the local fluid content, and $\delta u / u$ denotes the relative error of the flow velocity. For the PDMS microvascular model, the error of flow velocity mainly originates from the measurement error for the temperature as the fluid content can

be accurately calculated. For tissues, the variation of fluid (blood) content for different tissues also contributes to the measurement error. Previous reports indicate $s = 4\% \pm 1\%$ for the muscle, and $29\% \pm 4\%$ for the kidney (Linderkamp et al., 1980).

2.5. In vitro evaluation of sensor performance

Hot-pulling polyvinyl alcohol (PVA) from a filament-type 3D printer formed PVA wires of $\sim 100 \mu\text{m}$ diameter. Confining multiple PVA wires (the ends of the wires were tied outside the mold) in a mold, filling PDMS precursors (Sylgard 184), and curing the PDMS defined the structures for the microvascular model. Immersion in water (75°C , water changed daily) dissolved the PVA and left channels of $\sim 100 \mu\text{m}$ diameter. Kwik-Sil (World Precision Instruments) silicone glue bonded the flow probe to the surface of this microvascular model. A syringe pump induced flow of water into the channels at a well-defined flow rate. Note that demounting and remounting the flow probe on the PDMS microvascular model could introduce changes of effective thermal conductivity k ; as such, Figs. 2 and 3 (in vitro test) only show the result from one representative flow probe. Either a wired system (a voltage source and a switching unit, Agilent 34970A/34901A) or a wireless BLE module powered the heater and measured the resistance of the

thermistors. An optional infrared camera (FLIR) also monitored the temperature distribution around the heater. Using least square fitting with the temperature measured by the thermistors (ΔT) and the distances between the thermistors and the heater (r) for the analytical model yielded flow velocity u . Parameters (room temperature) used in the analytical model were: $R = 0.75 \text{ mm}$, $k_{\text{water}} = 0.6 \text{ W m}^{-1}\text{K}^{-1}$, $k_{\text{isopropanol,70 wt\%}} = 0.28 \text{ W m}^{-1}\text{K}^{-1}$, $k_{\text{PDMSflapmodel}} = 0.27 \text{ W m}^{-1}\text{K}^{-1}$, $k_{\text{probe}} = 1.82 \text{ W m}^{-1}\text{K}^{-1}$, $s = 2.5\%$, $\alpha = 0.12 \text{ mm}^2 \text{ s}^{-1}$.

2.6. In vitro barb degradation test

Immersing the CA barbed cladding structures on the flow probes in phosphate buffered saline (PBS) at 37°C served as the basis for in vitro tests of barb degradation. Inserting probes with CA barbs in gelatin gels (from porcine skin, 10 wt% in water) allowed for characterization of their hooking properties. Determining the maximum force necessary to pull out the probe involved pulling with a force gauge (Mark 10). Applying mechanical disturbances by pulling and wiggling the copper wire/silicone tube cable enabled tests of the stability of the sensor under harsh mechanical conditions.

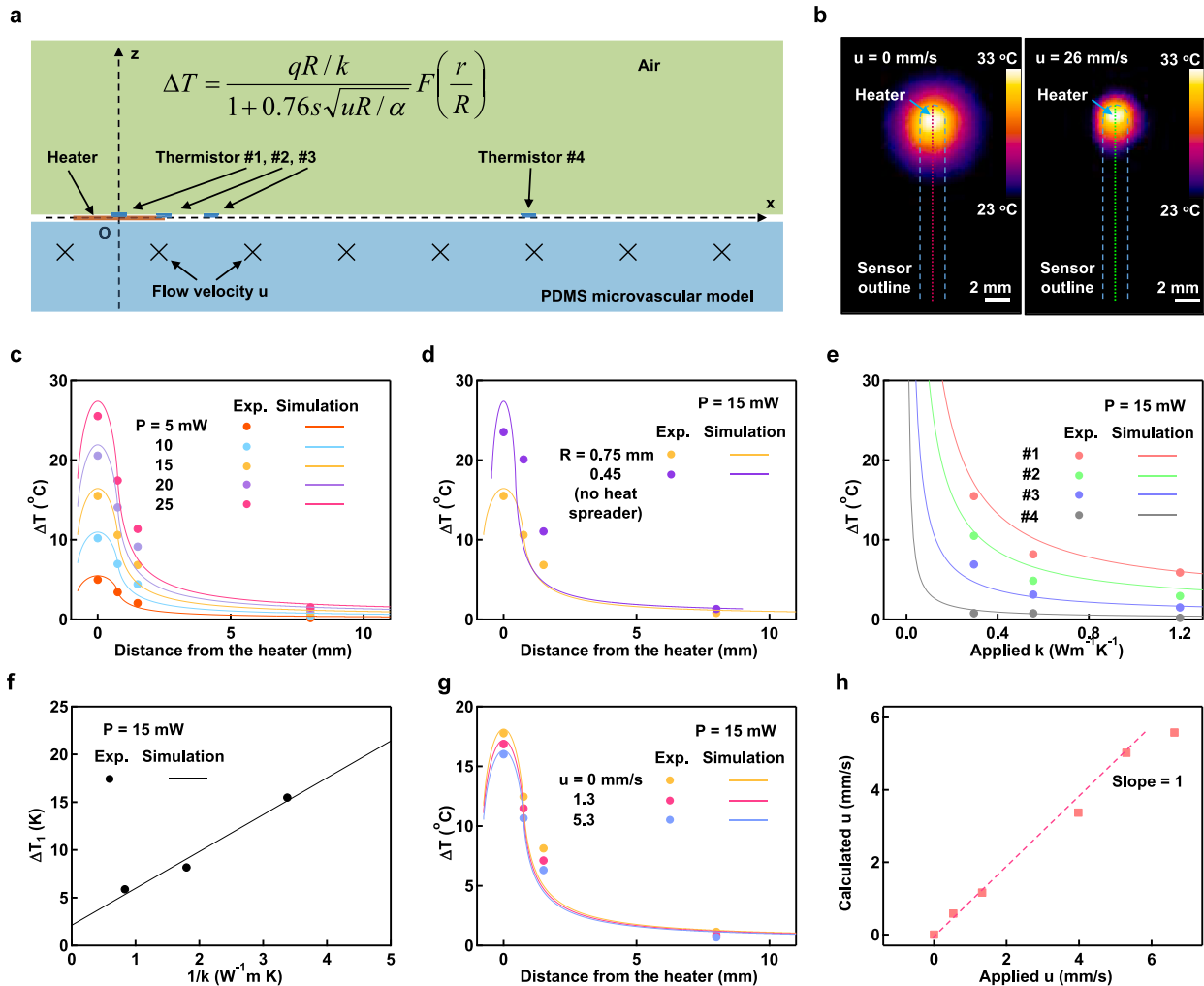


Fig. 2. a) Schematic illustration of the in vitro flow sensing setup (a flow probe mounted on a PDMS microvascular model) used to verify analytical models of the measurement physics. b) Temperature distribution around a flow probe mounted on a PDMS model with and without the presence of the microvascular flow. c)-e) Temperature increase measured by the thermistors (ΔT) compared with results computed using the analytical model, c) at different heater power; d) with and without the heat spreader and e) in different media. f) Plot that shows a linear relationship between ΔT of the 1st thermistor (ΔT_1) and the inverse thermal conductivity of the media. g) Plot that compares ΔT with simulated results at different flow velocities. h) Plot that compares flow velocity calculated from the analytical model with the actual applied velocity.

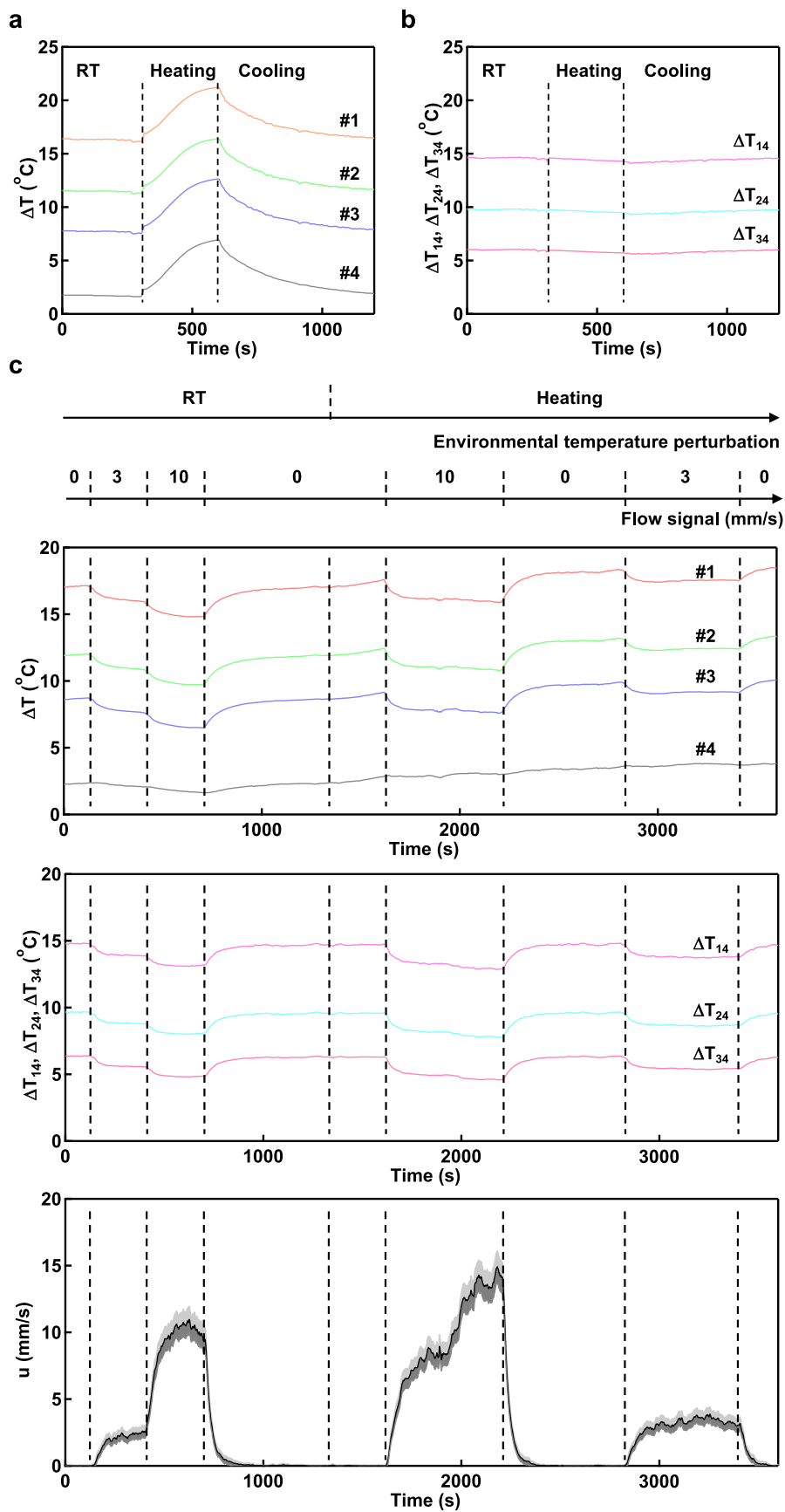


Fig. 3. a) Temperature increase measured by the thermistors (ΔT) when changing the temperature of the environment. b) Temperature difference between the thermistors when changing the temperature of the environment. c) Calculation of flow velocity when changing the temperature of the environment. Shaded curves denote the uncertainty in the flow velocity.

2.7. In vivo biocompatibility study

Animal procedures were performed in compliance with guidelines set by the Washington University Institutional Animal Use and Care Committee and the National Institutes of Health. Adult male Lewis rats (250 g, Charles River Laboratories, Wilmington, MA) were housed in a central animal care facility at 72 °F and a humidity between 30% and 70% on a standard 12 h light - 12 h dark cycle. Food (PicoLab rodent diet 20, Purina Mills Nutrition International, St. Louis, MO) and water were provided *ad libitum*. The animals were monitored postoperatively for signs of infection and distress before and after surgery.

After anesthesia (inducing with 4% and maintaining at 2% isoflurane) and sterilization, making a 2-mm skin slot at distal end of right hind leg exposed the gastrocnemius muscle. The implantation started with making a tunnel in the gastrocnemius muscle, followed by inserting the CA barb with tweezers. Closing the muscle and skin with one stitch using 4-0 nylon suture finished the surgery.

At 4 weeks post-surgery, harvesting rat gastrocnemius muscles (~5 × 10 × 10 mm³) after euthanasia of both operated and unoperated sides prepared the tissues as experimental and control groups, respectively. Preparing for histological analysis started with fixing tissues with 10% neutral buffered formalin and embedding them in paraffin wax, followed by transverse and longitudinal sectioning to micrometer-thick and standard protocols for H&E staining. Sections were imaged by a microscope (Keyence) with bright-field mode.

2.8. In vivo evaluation of sensor performance in porcine models

Animal research was performed with approval of the Institutional Animal Care and Use Committee at Washington University School of Medicine. This was performed as per U.S. Department of Agriculture Animal Welfare Regulations at an accredited facility. 3 live pigs were utilized for this study. Anesthesia was induced with telazol, ketamine, and xylazine followed by maintenance with inhaled isoflurane. After completion of all experimentation, the animal was euthanized with pentobarbital.

A left pedicled rectus abdominis myocutaneous flap was raised based upon the deep superior epigastric artery and veins in addition to the superficial superior epigastric vein (Fig. 5). To deploy the intramuscular

probe, a 15# blade was used to make stab incision oriented along the axis of the muscle fibers on the undersurface of the rectus abdominis muscle, being careful to avoid the pedicle vessels. The probe was then inserted into the muscle pocket. The entire deployment procedure took less than 30 s. The flap was restored to its anatomic orientation and the intramuscular probe was connected to its external processor via Bluetooth. A ViOptix T.Ox probe was adhered to the central portion of the skin paddle and then attached to the external monitor via the fiberoptic cable. Each myocutaneous flap was monitored continuously throughout the experiment using both devices in parallel.

After achieving a stable baseline reading for each device for 15 min, an Acland clamp was applied to the right deep superior epigastric artery to induce complete ischemia. Ischemia was maintained for 15 min. The Acland clamp was then released and 15 min were then allowed for flap recovery and re-establishment of a stable baseline reading. Acland clamps were then applied to the deep and superficial superior epigastric veins in order to induce venous congestion. Congestion was maintained for 15 min. The Acland clamps were then released, and 15 min were then allowed for flap recovery and re-establishment of a stable baseline reading. This experiment was then replicated using used probes, for separate animals on separate days to demonstrate reproducibility.

The peritoneal cavity was accessed through a laparotomy incision. The small bowel was retracted, and the posterior peritoneum was incised over the left kidney and renal vessels. The kidney was separated from all surrounding tissues bluntly, and isolated upon the renal vein, renal artery, and the ureter. Vessel loops were double-looped around the artery and vein to allow intermittent and atraumatic occlusion. The sensor was deployed within the kidney by puncturing its capsule with a #11 blade. The probe was advanced bluntly through this capsular rent, where it was quite stable. After establishment of a flow baseline, renal artery thrombosis was simulated by placing tension on the vessel loop encircling the artery. Ischemia was confirmed by obvious pallor of the organ. After 15 min, the vessel loop was loosened, and perfusion was re-established. After 15 min, a similar procedure was used to simulated renal vein thrombosis, and congestion was confirmed by observing purple discoloration of the organ. After 15 min venous occlusion was released, and reperfusion was allowed.

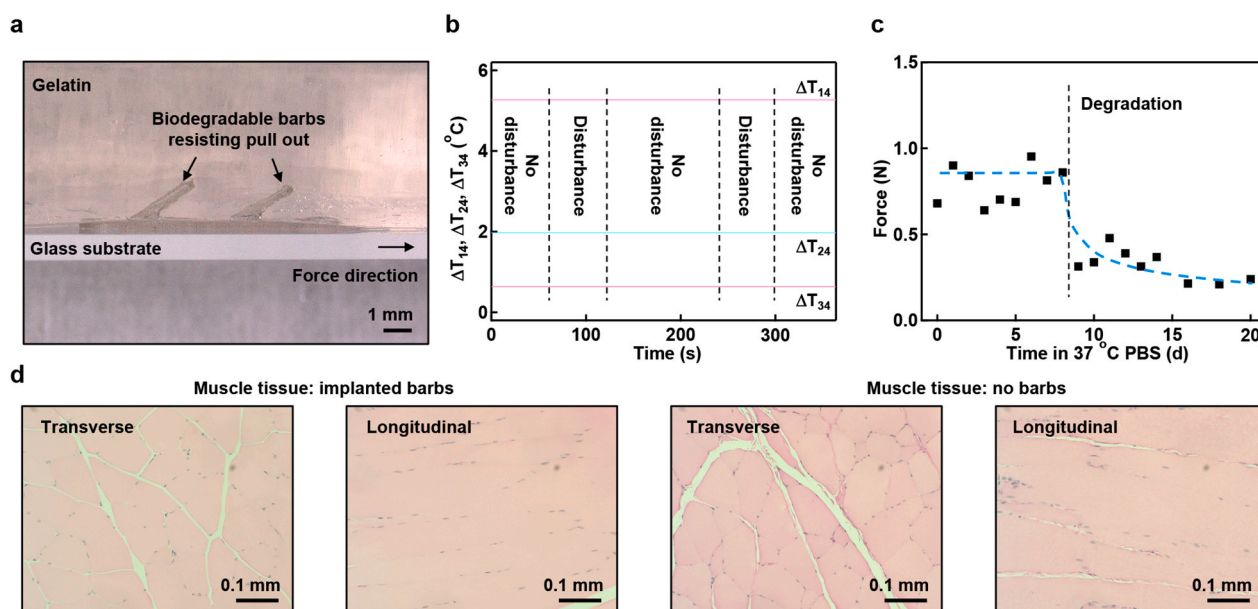


Fig. 4. a) Hooking mechanism associated with the biodegradable bars. b) Temperature difference between the thermistors when applying mechanical disturbances. c) Force for extracting the probe cladded with bars as a function of time in phosphate buffered saline at 37 °C. d) Histology of rat muscle tissues implanted with biodegradable bars, together with the control group.

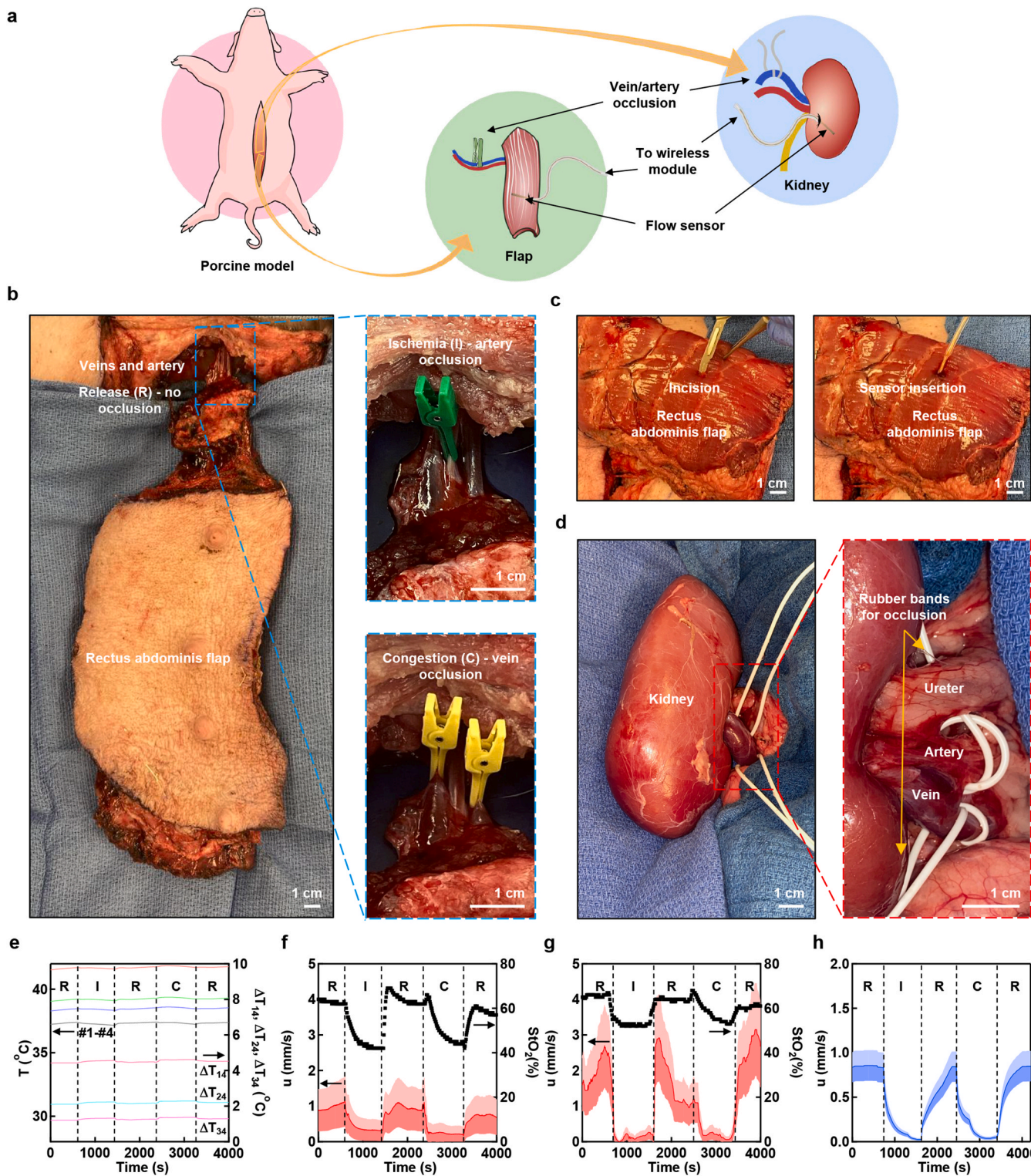


Fig. 5. a) Schematic illustration of flow sensing in a flap and an organ (kidney) in a porcine model. b) left, photograph of a rectus abdominis flap with isolated veins and artery; right, clamps on a vein and artery to control the blood flow in the flap. c) Probe implantation process. d) left, photograph of a kidney; right, rubber bands on vein and artery to control the blood flow in the kidney. e) Absolute temperature of the thermistors and temperature difference between the thermistors for a rectus abdominis flap measured in release (R) and artery/vein occluded (I/C) conditions. f) Measured microvascular flow velocity and StO_2 for the case of e. g) Results for the same sensor in f, but for another flap in a different porcine model. h) Measured microvascular flow velocity in a kidney. Shaded curves denote the error of the flow velocity.

3. Results

3.1. Verification of the flow sensing theory

A microvascular model enables quantitative verification of this expression (Fig. 2a). The model consists of microchannels (~100 μm diameter) of random orientations (Fig. S3, Methods section) embedded in a PDMS matrix, with channel volume percentage $s \sim 2.5\%$. An infrared camera reveals the circular symmetry of the temperature distribution that results from operation. The absence of any spatial asymmetry in ΔT suggests that the contributions of 1) heat conduction by the metal traces, the substrate and the encapsulation layer, and 2) heating effects by passing a high current through the metal traces connected to the heater are both negligible in our design. Introducing flow into the model reduces the increase in the temperature of the local environment, as anticipated by Equation (2) (Fig. 2b). Temperatures measured by the device serve as the basis for quantitative validation of these and other effects. Without flow, the temperature distribution is proportional to the heater power $P = q\pi R^2$, consistent with Equation (2) (Fig. 2c). Comparing the performance with and without the circular heat spreader indicates that the spreader reduces the peak temperature and broadens the distribution (Fig. 2d). Increasing the effective heater radius by adding the heat spreader also boosts the relative sensitivity of the sensor (Equation (2)). Immersing the probe in media with different thermal conductivities such as isopropanol (70 wt%) and water verifies the linear relationship between the temperature and the inverse of the effective thermal conductivity of the media $1/k$ (Fig. 2e and f). Here the non-zero intercept (Fig. 2f) results from the small but finite effective thermal conductivity of the materials in the probe, mainly the encapsulation. This is because the limit $u = 0$ in Equation (2) provides a way to determine and calibrate the effective thermal conductivity k , accounting for effects of encapsulation layers between the heater/sensors and tissue, and metal wires on the surface, underneath and outside the heater (Supplementary Note 1). Finally, the flow decreases the temperature at different distances from the heater (Fig. 2g), such that the flow velocity u can be determined from ΔT , with values that agree well with the known applied velocities (Fig. 2h).

3.2. Robustness of the results against thermal or mechanical fluctuations

For robust operation, the design of the sensor should minimize effects of fluctuations in the surrounding temperature. Analyzing the temperature differences between thermistors (ΔT_{14} , ΔT_{24} , ΔT_{34}) rather than ΔT greatly reduces these effects. Specifically, ΔT_{14} , ΔT_{24} , and ΔT_{34} are almost invariant to changes in temperature of the surroundings, even for magnitudes ($\sim 5^\circ\text{C}$; Fig. 3a and b) much larger than those relevant to the application considered here. This reduction follows from similar effects of the surrounding temperature on ΔT from different thermistors. Experimental measurements of flow under changing surrounding temperature confirm this expectation (Fig. 3c).

Biodegradable barbs of cellulose acetate (CA) form a cladding layer (thickness 250 μm) on the probe, as described previously. CA is a non-toxic structural material used in implantable structures such as stents, designed to degrade in physiological conditions within a few months (Janjic et al., 2017). Inserting the barbs into transparent gelatin blocks of elastic modulus similar to biological tissues ($E \sim 70$ kPa for 10% gelatin (Karimi and Navidbakhsh, 2014), $E = 25$ –100 kPa for skeletal and cardiac muscles (Ogneva et al., 2010)) illustrates the hooking mechanism and demonstrates their mechanical characteristics (Fig. 4a). Mechanical perturbations generated by forces imparted to the probe through the flexible silicone cable of the sensor have negligible effects on the measured temperature differences (Fig. 4b). The force required to remove the probe from the incision reduces to ~ 0.3 N, abruptly after 9 d of immersion in simulated biofluid (phosphate buffered saline, PBS) at 37°C (Fig. 4c). Implanting the CA barb structures in skeletal muscle tissues of rat models confirms their biocompatibility. Histological

analysis shows an absence of neutrophils in the tissue surrounding the implanted barbs after 28 d (Fig. 4d).

3.3. In vivo performance

Implanting flow probes in porcine flap and organ models allow continuous, local monitoring of the microvascular flow velocity. The rectus abdominis myocutaneous flaps have dimensions of $30\text{ cm} \times 10\text{ cm} \times 2\text{ cm}$, with the three main veins and the main artery exposed (Fig. 5a). Clamping the corresponding vein and artery simulates the venous (“congested states”, C) and arterial thrombosis (“ischemia states”, I) states, respectively, both of which stop microvascular blood flow and immediately threaten flap viability (Fig. 5b). The implantation involves incising the flap with a scalpel (~ 2 cm deep) and inserting the flow probe (Fig. 5c). Similar procedures enable flow measurements from the kidney (Fig. 5d). For the flap, compared to the states without clamping the vein or the artery (“release states”, R), both I and C states show significant increases in ΔT_{14} , ΔT_{24} and ΔT_{34} (Fig. 5e). Converting these temperature differences into flow velocities using Equation (2) yields a clear difference between the I and C states (0.3 ± 0.3 and 0.2 ± 0.2 mm/s, 1.2 ± 1.2 and 0.8 ± 0.8 mL/100 mL min) and the R state (1.0 ± 0.6 mm/s, 4.1 ± 2.4 mL/100 mL min, Fig. 5f) even accounting for the increased measurement error, which mainly originates from the uncertainty of the blood percentage s in muscles (Methods section), compared with the benchtop measurements on the PDMS microvascular model (Linderkamp et al., 1980). The flow velocity and perfusion of the R state is also consistent with previous values determined by direct imaging (0.5–1.5 mm/s in the capillary vessels in brain of a rabbit (Ivanov et al., 1981) and electromagnetic blood flowmetry (3.8–8.0 mL/100 mL min in canine and feline muscles) (Clarke and McKee, 1991). Furthermore, the time that characterizes the transition between the flow and no flow states (1–5 min) is comparable to that associated with measurements of StO_2 captured using commercial devices mounted on the skin (Fig. 5f). Such characterizing time is also similar to the response time of the individual NTC temperature sensors to external temperature stimuli (Fig. 3a), also suggesting that the flow probes are able to respond rapidly to the change of flow states. The temperature increase of the probe (heating power 10 mW) is less than 4°C (Fig. 5e), safe for clinical use in tissues without enhanced thermal sensitivity (tissues excluding the eyes and those in the nervous or reproductive system), according to a guidance from United States Food and Drug Administration (2021). Decreasing the heating power may further reduce the increase in the temperature of the probe. The absolute magnitude of the change in temperature does not affect the flow measurement, as expected (Fig. 5d). Reuse of the flow sensor is possible by replacing the biodegradable barb cladding structure. The same device yields similar flow velocities u (2.0 ± 0.9 , 0.2 ± 0.1 and 0.2 ± 0.1 mm/s) and perfusion w (8.2 ± 3.7 , 0.8 ± 0.4 and 0.8 ± 0.4 mL/100 mL min) for the R, I and C states in a flap from another porcine model (Fig. 5g). Variation in these values are likely due to the variation of the blood content s in different muscle tissues of different animals. Similar results from Fig. 2f and g also suggest that the performance of the flow probes is still stable after repetitive flow state changes. Different flow probes implanted in different porcine models also show negligible differences of sensing results (Fig. S5). Again, for the kidney model, values for ΔT and the flow velocity respond rapidly to clamping events (Fig. 5h). The values of u (0.9 ± 0.2 , 0.03 ± 0.01 and 0.04 ± 0.01 mm/s) for the R, I and C states are also similar to those measured in the flaps, and the values of perfusion w in R states (35 ± 11 mL/100 mL min) are similar to those in transplanted kidneys (Notohamiprodjo et al., 2016).

4. Discussion and conclusion

The results presented here indicate that this sensing platform can reliably monitor the microvascular flow velocities in flaps and organ grafts for transplantation, in a manner that is robust to changes in

temperature of the tissue. The biodegradable barbs ensure mechanically stable positioning and they greatly simplify the extraction process. Compared with previous flow sensors, this technology eliminates bulky readout instruments and related mechanical artifacts in the measurement results. The use of standard smartphones for control, data acquisition, display and analysis reduce the cost of the system and facilitates routine use. Additionally, multiple temperature sensors reduce measurement errors and laser-processed ultrathin metal interconnects minimize parasitic thermal transport through the probe, for accurate measurements of flow. Compared to the physical models reported previously focusing on spherical heaters, the model introduced here employs 2-dimensional (2D) circular heaters, enabling the design of sensors implemented with heat spreaders, which enhances the relative sensitivity of the sensor. Pre-defined calibrations (Supplementary Note 1) eliminate the effects of thermal contact resistances. In muscle flaps and kidneys of porcine models, the measured flow velocities (0.9–2.0 mm/s) and perfusion (4.1–8.2 mL/100 mL min for flaps, 35 mL/100 mL min for kidneys) are both similar to microscopic (by direct imaging) and macroscopic characteristics (by blood flowmetry) observed in previous reports, and the response to simulated venous and arterial thrombosis is fast (1–5 min). In the future, integration with other sensors such as those for StO₂ will yield additional information and mitigate uncertainties associated with variations in the blood content *s*. Similar probes constructed using fully biodegradable materials may completely eliminate the necessity of removal, further simplifying the related clinical protocols. Long-term animal tests could also yield the lifetime of the flow probe in biological environments. These features and associated future possibilities suggest that this overall measurement approach may lead to routine, quantitative means for evaluating the health status of transplanted tissues, giving key early indicators of thrombosis and related adverse events in practical clinical applications.

CRediT authorship contribution statement

Di Lu: Experiment design, flow sensor fabrication, data acquisition, Formal analysis, Writing – original draft, Writing – review & editing. **Shupeng Li:** Experiment design, theoretic model, Writing – original draft, Writing – review & editing. **Quansan Yang:** Experiment design, flow sensor fabrication, data acquisition, Writing – review & editing. **Hany M. Arafa:** BLE module, Writing – review & editing. **Yameng Xu:** Data acquisition, biocompatibility surgery, Writing – review & editing. **Ying Yan:** Biocompatibility surgery, Writing – review & editing. **Diana Ostojich:** BLE module, Writing – review & editing. **Wubin Bai:** Data acquisition, Writing – review & editing. **Hexia Guo:** Data acquisition, Writing – review & editing. **Changsheng Wu:** Data acquisition, Writing – review & editing. **Shuo Li:** Data acquisition, Writing – review & editing. **Lauren Jacobson:** Flow model surgery, Writing – review & editing. **Amanda M. Westman:** Flow model surgery, Writing – review & editing. **Matthew R. MacEwan:** Biocompatibility surgery, Writing – review & editing. **Yonggang Huang:** Experiment design, theoretic model, Writing – original draft, Writing – review & editing. **Mitchell Pet:** Experiment design, flow model surgery, Writing – original draft, Writing – review & editing. **John A. Rogers:** Experiment design, Writing – original draft, Writing – review & editing.

Declaration of competing interest

The authors declare that they have no known competing financial interests or personal relationships that could have appeared to influence the work reported in this paper.

Acknowledgments

This work utilized Northwestern University Micro/Nano Fabrication Facility (NUFAB) of Northwestern University's NUANCE Center, which has received support from Soft and Hybrid Nanotechnology

Experimental (SHyNE) Resource (NSF ECCS-1542205), the Materials Research Science and Engineering Center (NSF DMR-1720139) at the Materials Research Center, the International Institute for Nanotechnology (IIN), the Keck Foundation, the State of Illinois through the IIN, and Northwestern University, and the Querrey-Simpson Institute for Bioelectronics.

Appendix A. Supplementary data

Supplementary data to this article can be found online at <https://doi.org/10.1016/j.bios.2022.114145>.

References

- Administration, U.S.F.a.D., 2021. Testing and Labeling Medical Devices for Safety in the Magnetic Resonance (MR) Environment.
- Amdisen, C., Jespersen, B., Moldrup, U., Keller, A.K., 2017. The unsuitability of implantable Doppler probes for the early detection of renal vascular complications - a porcine model for prevention of renal transplant loss. *PLoS One* 12 (5), e0178301.
- Anderson, G.T., Valvano, J.W., Santos, R.R., 1992. Self-heated thermistor measurements of perfusion. *IEEE Trans. Biomed. Eng.* 39 (9), 877–885.
- Arkin, H., Xu, L.X., Holmes, K.R., 1994. Recent developments in modeling heat transfer in blood perfused tissues. *IEEE Trans. Biomed. Eng.* 41 (2), 97–107.
- Askari, M., Fisher, C., Weniger, F.G., Bidic, S., Lee, W.P., 2006. Anticoagulation therapy in microsurgery: a review. *J. Hand. Surg. Am.* 31 (5), 836–846.
- Baish, J.W., 2015. Molecular, cellular, and tissue engineering. In: Bronzino, J.D., Peterson, D.R. (Eds.), *Molecular, Cellular, and Tissue Engineering*. CRC Press.
- Bergman, T.L., Incropera, F.P., DeWitt, D.P., Lavine, A.S., 2011. *Fundamentals of Heat and Mass Transfer*. John Wiley & Sons, Hoboken, NJ, USA.
- Bhagat, V., Becker, M.L., 2017. Degradable adhesives for surgery and tissue engineering. *Biomacromolecules* 18 (10), 3009–3039.
- Carslaw, H.S., Jaeger, J.C., 1959. *Conduction of Heat in Solids*. Clarendon Press, Oxford, UK.
- Chen, K.T., Mardini, S., Chuang, D.C., Lin, C.H., Cheng, M.H., Lin, Y.T., Huang, W.C., Tsao, C.K., Wei, F.C., 2007. Timing of presentation of the first signs of vascular compromise dictates the salvage outcome of free flap transfers. *Plast. Reconstr. Surg.* 120 (1), 187–195.
- Chen, M.M., Holmes, K.R., Rupinkas, V., 1981. Pulse-decay method for measuring the thermal conductivity of living tissues. *J. Biomech. Eng.* 103 (4), 253–260.
- Chung, H.U., Rwei, A.Y., Hourlier-Fargette, A., Xu, S., Lee, K., Dunne, E.C., Xie, Z., Liu, C., Carlini, A., Kim, D.H., Ryu, D., Kulikova, E., Cao, J., Odland, I.C., Fields, K.B., Hopkins, B., Banks, A., Ogle, C., Grande, D., Park, J.B., Kim, J., Irie, M., Jang, H., Lee, J., Park, Y., Kim, J., Jo, H.H., Hahm, H., Avila, R., Xu, Y., Namkoong, M., Kwak, J.W., Suen, E., Paulus, M.A., Kim, R.J., Parsons, B.V., Human, K.A., Kim, S.S., Patel, M., Reuther, W., Kim, H.S., Lee, S.H., Leedle, J.D., Yun, Y., Rigali, S., Son, T., Jung, I., Arafa, H., Soundararajan, V.R., Ollech, A., Shukla, A., Bradley, A., Schau, M., Rand, C.M., Marsillio, L.E., Harris, Z.L., Huang, Y., Hamvas, A., Paller, A. S., Weese-Mayer, D.E., Lee, J.Y., Rogers, J.A., 2020. Skin-interfaced biosensors for advanced wireless physiological monitoring in neonatal and pediatric intensive-care units. *Nat. Med.* 26 (3), 418–429.
- Clarke, H.M., McKee, N.H., 1991. Perfusion parameters and pressure at zero flow in canine gracilis muscle flaps. *J. Surg. Res.* 51 (5), 409–412.
- Diller, K.R., 2017. Bioheat transfer. In: Chhabra, R.P. (Ed.), *CRC Handbook of Thermal Engineering Second Edition*, second ed. CRC Press.
- Hirigoyen, M.B., Urken, M.L., Weinberg, H., 1995. Free flap monitoring: a review of current practice. *Microsurgery* 16 (11), 723–726.
- Ivanov, K.P., Kalinina, M.K., Levkovich, Y.I., 1981. BLOOD-FLOW velocity IN capillaries OF brain and muscles and its physiological significance. *Microvasc. Res.* 22 (2), 143–155.
- Jaeger, M., Soehle, M., Schuhmann, M.U., Winkler, D., Meixensberger, J., 2005. Correlation of continuously monitored regional cerebral blood flow and brain tissue oxygen. *Acta Neurochir.* 147 (1), 51–56 discussion 56.
- Janjic, M., Pappa, F., Karagkiozaki, V., Gitas, C., Ktenidis, K., Logothetidis, S., 2017. Surface modification of endovascular stents with rosuvastatin and heparin-loaded biodegradable nanofibers by electrospinning. *Int. J. Nanomed.* 12, 6343–6355.
- Kang, S.K., Murphy, R.K., Hwang, S.W., Lee, S.M., Harburg, D.V., Krueger, N.A., Shin, J., Gamble, P., Cheng, H., Yu, S., Liu, Z., McCall, J.G., Stephen, M., Ying, H., Kim, J., Park, G., Webb, R.C., Lee, C.H., Chung, S., Wie, D.S., Gujar, A.D., Vemulapalli, B., Kim, A.H., Lee, K.M., Cheng, J., Huang, Y., Lee, S.H., Braun, P.V., Ray, W.Z., Rogers, J.A., 2016. Bioresorbable silicon electronic sensors for the brain. *Nature* 530 (7588), 71–76.
- Karimi, A., Navidbakhsh, M., 2014. Material properties in unconfined compression of gelatin hydrogel for skin tissue engineering applications. *Biomed. Eng.-Biomed. Tech.* 59 (6), 479–486.
- Keller, A., 2007. Noninvasive tissue oximetry for flap monitoring: an initial study. *J. Reconstr. Microsurg.* 23 (4), 189–197.
- Keller, A., 2009. A new diagnostic algorithm for early prediction of vascular compromise in 208 microsurgical flaps using tissue oxygen saturation measurements. *Ann. Plast. Surg.* 62 (5), 538–543.
- Khot, M.B., Maitz, P.K., Phillips, B.R., Bowman, H.F., Pribaz, J.J., Orgill, D.P., 2005. Thermal diffusion probe analysis of perfusion changes in vascular occlusions of rabbit pedicle flaps. *Plast. Reconstr. Surg.* 115 (4), 1103–1109.

- Kobayashi, K., Censullo, M.L., Rossman, L.L., Kyriakides, P.N., Kahan, B.D., Cohen, A.M., 2007. Interventional radiologic management of renal transplant dysfunction: indications, limitations, and technical considerations. *Radiographics* 27 (4), 1109–U1143.
- Kozusko, S., Gbulie, U., 2018. Detecting microsurgical complications with ViOptix tissue oximetry in a pediatric myocutaneous free flap: case presentation and literature review. *J. Reconstr. Microsurg. Open* 3 (1), e8–e12.
- Krishnan, S.R., Arafa, H.M., Kwon, K., Deng, Y., Su, C.J., Reeder, J.T., Freudman, J., Stankiewicz, I., Chen, H.M., Loza, R., Mims, M., Mims, M., Lee, K., Abecassis, Z., Banks, A., Ostojich, D., Patel, M., Wang, H., Börekçi, K., Rosenow, J., Tate, M., Huang, Y., Alden, T., Potts, M.B., Ayer, A.B., Rogers, J.A., 2020. Continuous, noninvasive wireless monitoring of flow of cerebrospinal fluid through shunts in patients with hydrocephalus. *NPJ Digital Med.* 3, 29.
- Kroll, S.S., Schusterman, M.A., Reece, G.P., Miller, M.J., Evans, G.R.D., Robb, G.L., Baldwin, B.J., 1996. Timing of pedicle thrombosis and flap loss after free-tissue transfer. *Plast. Reconstr. Surg.* 98 (7), 1230–1233.
- Kwon, K., Wang, H., Lim, J., Chun, K.S., Jang, H., Yoo, I., Wu, D., Chen, A.J., Gu, C.G., Lipschultz, L., Kim, J.U., Kim, J., Jeong, H., Luan, H., Park, Y., Su, C.J., Ishida, Y., Madhvapathy, S.R., Ikoma, A., Kwak, J.W., Yang, D.S., Banks, A., Xu, S., Huang, Y., Chang, J.K., Rogers, J.A., 2021. Wireless, soft electronics for rapid, multisensor measurements of hydration levels in healthy and diseased skin. *Proc. Natl. Acad. Sci. U. S. A.* 118 (5).
- Lee, K., Ni, X., Lee, J.Y., Arafa, H., Pe, D.J., Xu, S., Avila, R., Irie, M., Lee, J.H., Easterlin, R.L., Kim, D.H., Chung, H.U., Olabisi, O.O., Getaneh, S., Chung, E., Hill, M., Bell, J., Jang, H., Liu, C., Park, J.B., Kim, J., Kim, S.B., Mehta, S., Pharr, M., Tzavelis, A., Reeder, J.T., Huang, L., Deng, Y., Xie, Z., Davies, C.R., Huang, Y., Rogers, J.A., 2020. Mechano-acoustic sensing of physiological processes and body motions via a soft wireless device placed at the suprasternal notch. *Nat. Biomed. Eng.* 4 (2), 148–158.
- Linderkamp, O., Berg, D., Betke, K., Kofler, F., Krieger, H., Riegel, K.P., 1980. BLOOD-VOLUME And hematocrit IN various organs IN newborn piglets. *Pediatr. Res.* 14 (12), 1324–1327.
- Lorenzetti, F., Salmi, A., Ahovuo, J., Tukiainen, E., Asko-Seljavaara, S., 1999. Postoperative changes in blood flow in free muscle flaps: a prospective study. *Microsurgery* 19 (4), 196–199.
- Lu, W., Bai, W.B., Zhang, H., Xu, C.K., Chiarelli, A.M., Vazquez-Guardado, A., Xie, Z.Q., Shen, H.X., Nandoliya, K., Zhao, H.B., Lee, K., Wu, Y.X., Franklin, D., Avila, R., Xu, S., Rwei, A., Han, M.D., Kwon, K., Deng, Y.J., Yu, X.G., Thorp, E.B., Feng, X., Huang, Y.G., Forbess, J., Ge, Z.D., Rogers, J.A., 2021. Wireless, implantable catheter-type oximeter designed for cardiac oxygen saturation. *Sci. Adv.* 7 (7), 14.
- Madhvapathy, S.R., Wang, H.L., Kong, J., Zhang, M., Lee, J.Y., Bin Park, J., Jang, H.Y., Xie, Z.Q., Cao, J.Y., Avila, R., Wei, C., D'Angelo, V., Zhu, J.S., Chung, H., Coughlin, S., Patel, M., Winograd, J., Lim, J.M., Banks, A., Xu, S., Huang, Y.G., Rogers, J.A., 2020. Reliable, low-cost, fully integrated hydration sensors for monitoring and diagnosis of inflammatory skin diseases in any environment. *Sci. Adv.* 6 (49), 12.
- Notohamiprodjo, M., Kalnins, A., Andrassy, M., Kolb, M., Ehle, B., Mueller, S., Thomas, M.N., Werner, J., Guba, M., Nikolaou, K., Andrassy, J., 2016. Multiparametric functional MRI: a tool to uncover subtle changes following allogeneic renal transplantation. *PLoS One* 11 (11), e0165532.
- Novakovic, D., Patel, R.S., Goldstein, D.P., Gullane, P.J., 2009. Salvage of failed free flaps used in head and neck reconstruction. *Head Neck Oncol.* 1, 33.
- Ogneva, I.V., Lebedev, D.V., Shenkman, B.S., 2010. Transversal stiffness and young's modulus of single fibers from rat soleus muscle probed by atomic force microscopy. *Biophys. J.* 98 (3), 418–424.
- Pareja, E., Cortes, M., Navarro, R., Sanjuan, F., Lopez, R., Mir, J., 2010. Vascular complications after orthotopic liver transplantation: hepatic artery thrombosis. *Transplant. Proc.* 42 (8), 2970–2972.
- Park, Y., Kwon, K., Kwak, S.S., Yang, D.S., Kwak, J.W., Luan, H., Chung, T.S., Chun, K.S., Kim, J.U., Jang, H., Ryu, H., Jeong, H., Won, S.M., Kang, Y.J., Zhang, M., Pontes, D., Kampmeier, B.R., Seo, S.H., Zhao, J., Jung, I., Huang, Y.G., Xu, S., Rogers, J.A., 2020. Wireless, skin-interfaced sensors for compression therapy. *Sci. Adv.* 6 (49), 9.
- Poder, T.G., Fortier, P.H., 2013. Implantable Doppler in monitoring free flaps: a cost-effectiveness analysis based on a systematic review of the literature. *Eur. Ann. Otorhinolaryngol. Head Neck Dis.* 130 (2), 79–85.
- Rosenthal, G., Sanchez-Mejia, R.O., Phan, N., Hemphill 3rd, J.C., Martin, C., Manley, G. T., 2011. Incorporating a parenchymal thermal diffusion cerebral blood flow probe in bedside assessment of cerebral autoregulation and vasoreactivity in patients with severe traumatic brain injury. *J. Neurosurg.* 114 (1), 62–70.
- Rwei, A.Y., Lu, W., Wu, C., Human, K., Suen, E., Franklin, D., Fabiani, M., Gratton, G., Xie, Z., Deng, Y., Kwak, S.S., Li, L., Gu, C., Liu, A., Rand, C.M., Stewart, T.M., Huang, Y., Weese-Mayer, D.E., Rogers, J.A., 2020. A wireless, skin-interfaced biosensor for cerebral hemodynamic monitoring in pediatric care. *Proc. Natl. Acad. Sci. U. S. A.* 117 (50), 31674–31684.
- Seitz, J.M., Durisin, M., Goldman, J., Drelich, J.W., 2015. Recent advances in biodegradable metals for medical sutures: a critical review. *Adv. Healthc. Mater.* 4 (13), 1915–1936.
- Spiegel, J.H., Polat, J.K., 2007. Microvascular flap reconstruction by otolaryngologists: prevalence, postoperative care, and monitoring techniques. *Laryngoscope* 117 (3), 485–490.
- Valvano, J.W., Allen, J.T., Walsh, J.T., Hnatowich, D.J., Tomera, J.F., Brunengraber, H., Bowman, H.F., 1984. An isolated rat liver model for the evaluation of thermal techniques to quantify perfusion. *J. Biomech. Eng.* 106 (3), 187–191.
- Valvano, J.W., Cochran, J.R., Diller, K.R., 1985. Thermal conductivity and diffusivity of biomaterials measured with self-heated thermistors. *Int. J. Thermophys.* 6 (3), 301–311.
- Wykrzykowska, J.J., Kraak, R.P., Hofma, S.H., van der Schaaf, R.J., Arkenbout, E.K., Aj, I.J., Elias, J., van Dongen, I.M., Tijssen, R.Y.G., Koch, K.T., Baan Jr., J., Vis, M.M., de Winter, R.J., Piek, J.J., Tijssen, J.G.P., Henriques, J.P.S., Investigators, A., 2017. Bioresorbable scaffolds versus metallic stents in routine PCI. *N. Engl. J. Med.* 376 (24), 2319–2328.
- Yu, K.J., Kuzum, D., Hwang, S.W., Kim, B.H., Juul, H., Kim, N.H., Won, S.M., Chiang, K., Trumpis, M., Richardson, A.G., Cheng, H., Fang, H., Thomson, M., Bink, H., Talos, D., Seo, K.J., Lee, H.N., Kang, S.K., Kim, J.H., Lee, J.Y., Huang, Y., Jensen, F. E., Dichter, M.A., Lucas, T.H., Viventi, J., Litt, B., Rogers, J.A., 2016. Bioresorbable silicon electronics for transient spatiotemporal mapping of electrical activity from the cerebral cortex. *Nat. Mater.* 15 (7), 782–791.